J. Wind Eng. Ind. Aerodyn. ■ (■■■■) ■■■–■■■

Contents lists available at ScienceDirect

Journal of Wind Engineering and Industrial Aerodynamics

journal homepage: www.elsevier.com/locate/jweia

The role of corner vortices in dictating peak wind loads on tilted flat solar panels mounted on large, flat roofs

David Banks *

CPP Inc., 1415 Blue Spruce Drive, Fort Collins, CO 80524, USA

ARTICLE INFO

Keywords:
Roof corner vortices
Wind loads
Roof-mounted solar panels

ABSTRACT

Uplift wind loads on tilted flat PV panels mounted on the roofs of wide, rectangular, low-rise flat-roofed building were measured in an atmospheric boundary layer wind tunnel. The results indicate that for panels aligned with the building axes, the bubble separation that occurs for winds normal to a building face does not significantly increase these loads. Conversely, wind loads associated with the corner vortices are significantly higher than in the absence of the vortex. The direction of panel tilt relative to the vortex swirl, the position of the panel relative to the vortex reattachment, and the proximity of the panel to the vortex-originating corner together control the peak uplift. It is through changes to the vortices that the parapets affect wind loads. Vortex-related winds loads so dominate the uplift patterns on the roof that they need to be the primary consideration in any method designed to calculate these loads. This includes both experiments designed to study wind loads on this kind of PV racking system, and any calculation methods currently being codified in standards around the world.

1. Introduction

Very little information is available in the published literature concerning wind loads on roof-mounted solar panels, particularly tilted flat PV panels on large, flat roofs. Good wind load information is necessary to adequately assess the design and ballasting of such systems, which have been installed at hundreds if not thousands of sites around the world. This information can only be obtained from a suitable test procedure. The purpose of this paper is to provide guidance for such testing.

This paper summarizes the results of over 20 separate wind tunnel studies conducted at CPP to measure wind loads on a variety of racking systems in which tilted PV panels are placed in arrays on a flat-roofed building. The systems tested ranged in tilt from 0° to 25°, though the majority of tilts were between 5° and 15°. In all cases, they were positioned relatively close to the roof.

Fig. 1 illustrates a typical geometry and provides some nomenclature.

These wind tunnel studies are proprietary, and so details of the geometries tested cannot be provided in this paper. All testing was done in accordance with the requirements of Chapter 31 of ASCE 7-10 (ASCE, 2010). The author of this paper was the principal in charge of all tests, and all tests were conducted using similar methodologies, as detailed in section 2.

The results of these experiments, along with work conducted by Kopp et al. (2012), form the experimental basis for the wind load calculation procedures codified in the Structural Engineering Association of California (SEAOC) PV-2 2012 wind load guidelines for such systems (SEAOC, 2012). Several aspects of these procedures can be considered significant departures from how wind loads are calculated for the roof itself, including the size of the edge and corner zones, the influence of parapets, and the use of an effective tributary area that is normalized by the size of the building (see Kopp, in press). This paper discusses some of the wind loading patterns and trends which were common to all of the racking systems tested at CPP and which shaped the nature of these SEAOC PV2 procedures.

SEAOC PV2 2012 includes a section (31.6) on wind tunnel testing for wind loads on roof mounted solar panels which place restriction on how broadly applicable data from a specific test can be, and which mandates peer review of the testing and calculation procedures in some situations. As has been pointed out by Kopp and Banks (2013), these restrictions are necessary because building generated variations in the wind field acting on the array prevent the generalization of data from a single test configuration. In order to ensure a widely applicable wind tunnel test procedure, it is critical to understand how the building generated wind field acts on the array. This paper describes this interaction in detail, so that such a test can be designed.

As will be illustrated in the results section, the key to understanding this interaction is to examine the effects of the corner vortices. It is widely known that the worst wind loads on the roofs of low-rise, flat-roofed buildings occur near the roof edges, under the flow separation. In particular, the worst mean and peak suctions occur for cornering or oblique wind angles when corner vortices occur (Kind, 1986). For this reason, many building codes

* Tel.: +1 970 690 6959; fax: +1 970 221 3124.
E-mail address: dbanks@cppwind.com

0167-6105/$ - see front matter © 2013 Elsevier Ltd. All rights reserved.
http://dx.doi.org/10.1016/j.jweia.2013.08.015

Nomenclature

H	building height
W	building width
h_{pt}	parapet height
d	edge-to-edge row spacing
h_1	PV gap height above the roof
h_2	height of top of PV panel above the roof Dw, Ds, Sw, and Ss: vortex identifiers. See Fig. 7

and standards divide the roof into zones, and provide higher wind loading coefficients in the corner and along the edges (for example, ASCE 7-10).

It is perhaps therefore intuitive to expect that low-profile, tilted solar panels mounted on the roof should also be susceptible to the higher wind forces near the building edge than in the center of the roof, and that the roof zones would also be suitable for roof-mounted solar panels. The results presented in this paper demonstrate that this second assumption is not sound.

This study focuses on uplift loads necessary to calculate ballast for systems that are either not mechanically fastened, or are partially tied down, but still rely on weight to keep them from moving during a severe wind event. Downward-acting wind forces are not addressed.

2. Wind tunnel test methods

Wind tunnel testing of more than 20 different roof-mounted solar racking system designs was carried out in one of CPP's atmospheric boundary layer (ABL) wind tunnels. The wind tunnel has a 3 m-wide, 2.5 m tall test section. A range of approach flows were used, generally having exponents and turbulence typical of either suburban or open country approach flows. The most common approach flow was representative of an open country exposure, with a velocity profile exponent of 0.14, see Fig. 2.

The buildings ranged in height from 15 cm to 30 cm, and in width from 0.4 m to 2 m. Blockage ratios were kept below 7% in all tests. An image of a typical model building is presented in Fig. 3 where the width of the building (W) is six times greater than the height (H). The roof is divided into nine squares, shown in Fig. 4a, each $2H$ wide, and the array was placed in each of these locations for a separate test. In some cases, additional tests were run on a $2H \times 2H$ building, as shown in Fig. 4b. The turntable was rotated so that pressures were measured at wind direction increments of 10°.

A range of different pressure tap layouts have been used, depending on the scale of the model and the size of the solar assembly. A typical configuration had five or six taps on the upper surface and two on the lower surface of every panel in the array, for a total of over 600 taps in the array. Pressures were sampled

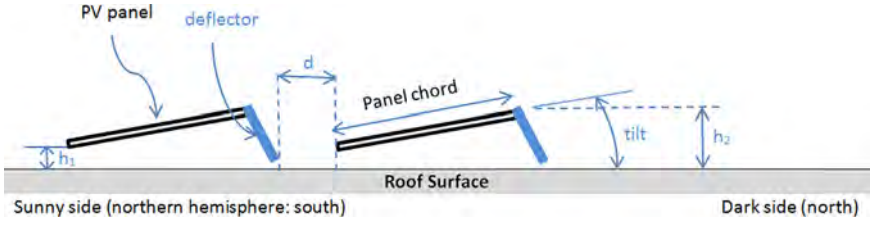

Fig. 1. Section of typical roof-mounted PV racking system geometry, with northern hemisphere conventions. In these tests, $h_1 < 2$ ft and $h_2 < 4$ ft. The roof tilt was 0° in all tests. Deflector as shown is stylized, and does not accurately represent any deflector tested in these experiments.

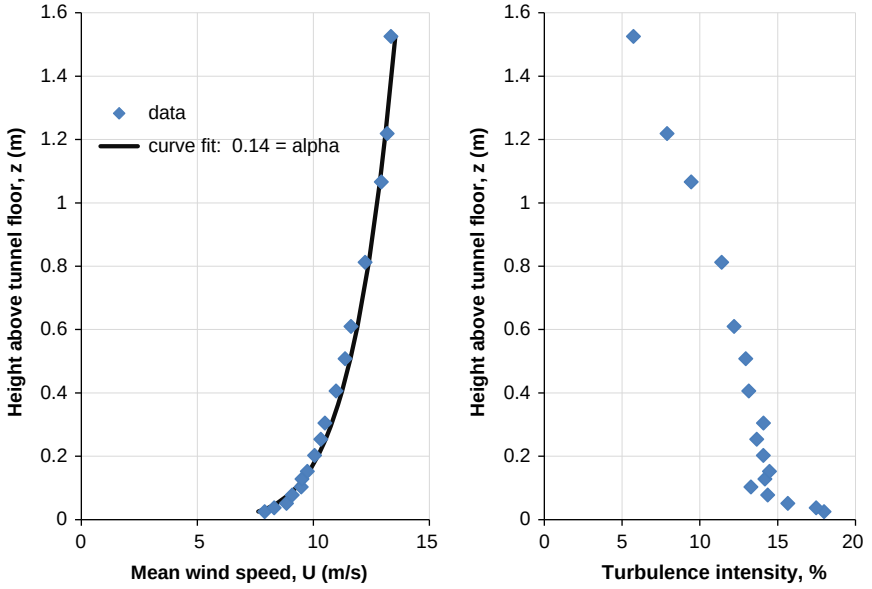

Fig. 2. Typical open country velocity profiles used in wind tunnel testing.

Please cite this article as: Banks, D., The role of corner vortices in dictating peak wind loads on tilted flat solar panels mounted on large, flat roofs. Journal of Wind Engineering & Industrial Aerodynamics (2013), http://dx.doi.org/10.1016/j.jweia.2013.08.015

simultaneously at all taps (both above and below the panels) at frequencies of either 250 Hz or 500 Hz for a periods ranging from 30 seconds to 2 minutes. A frequency domain correction was applied to account for the frequency response of the tubing-transducer system.

A typical array featured just over 100 panels in a square array, with pressures measured across every panel simultaneously. Panels were tested in both portrait and landscape orientation, and in both cases the roof corner vortices dominated the wind loading patterns. In all cases the height of the tops of the panels above the roof (h_2) was small in comparison to the height of the roof ($h_2 < 0.15h$).

In many cases wind deflectors were tested on the high side of the panels in order to reduce the wind uplift, and pressures were generally also measured across the deflectors. In cases where the deflectors provided significant shielding, taps were sometimes placed on the roof itself, rather than the underside of the panels. No data is presented in this paper regarding loads on the deflectors; all net pressures presented are area averaged net pressures across the panels only.

All data reported in this paper are from low profile systems, with an upper edge height above the roof under 1.2 m. Where geometric distortions such as solar panel thickness were necessary, priority was placed on matching gap sizing around the base and edges of the panels.

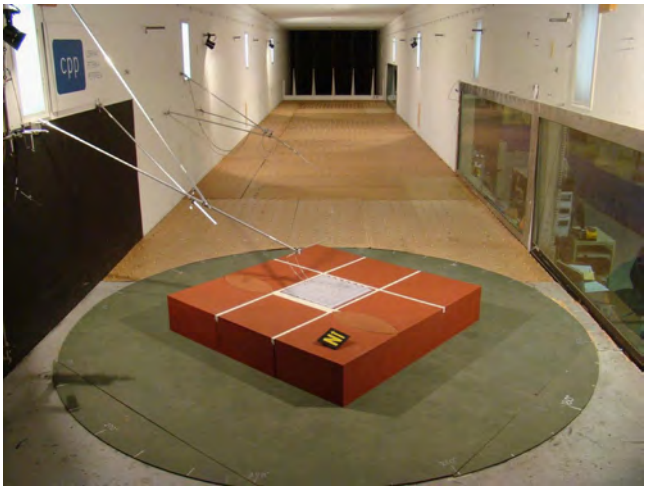

Fig. 3. Photo of a typical wind tunnel test to measure pressures on an array of solar panels. For this test, the array is positioned in the middle of a low rise building of height *H*. The building is square, with a side length of 6*H*. The array is tested in nine different roof positions.

Scales varied between 1:25 and 1:100, though over 80% of the tests were conducted at scales between 1:40 and 1:50. Due to the scaling of the models, it is impossible in the wind tunnel to reproduce the turbulence length scale associated with a full spectrum of energy in the full scale approach flow. The length scale in the tunnel is inevitably too small. In most tests, the high-frequency spectrum matching method was employed, as described by Banks (2011) and Dyrbye and Hansen (1997). This method matches the energy in the spectrum at frequencies above the quasi-steady threshold. GC_N values are calculated directly, using the following equation:

$$GC_N = p/q_z \tag{1}$$

where q_z is the velocity pressure of a 3-s gust at roof height, and p is the peak net uplift pressure across the entire panel, or in some cases, small groups of panels. This peak calculation method follows Richards et al. (2007) in dividing the peak pressure measured in the wind tunnel during a given interval by the gust velocity pressure measured during that same time interval.

Both the wind speed and pressure time series were divided into dozens of segments. The 3 s gust speed used to calculate q_z for each of these segments was determined by low-pass filtering the entire wind speed time series at a cutoff equivalent to 3 s of full scale time, and then finding the peak 3-s gust value for each time segment from this filtered time series. The GC_N values reported in this paper are the average of all of the GC_N values calculated for each segment.

The wind tunnel mean speed at a height of 0.5 m above the floor was typically 10 m/s, so that for most of our tests sample duration of 1 min corresponds to periods of between 10 and 15 min at full scale. All time conversions between full scale and model scale assumed a gust wind speed at full scale of 40 m/s and at a height of 10 m in an open country.

At scales of 1:100, the turbulence length scale was deemed to be close enough to what is required to match full scale (within a factor of 3) that peak pressure coefficients were measured and converted into gust pressures using a gust factor.

It is not the intent of this paper to compare the merits of these two methods of calculating GC_N in detail. It is possible that a comparison to full scale data is needed to determine which method is superior. However, all of the conclusions in this report relate to changes in loading as a function of the position of the panels on the roof and of the shape of the building. The vortex dominated loading pattern presented in the results section below were present for all experiments, regardless of pressure tap layouts, approach flows, panel tilts, and array model scales, and were observed for both GC_N calculation methods. It is the intent of this paper to provide enough

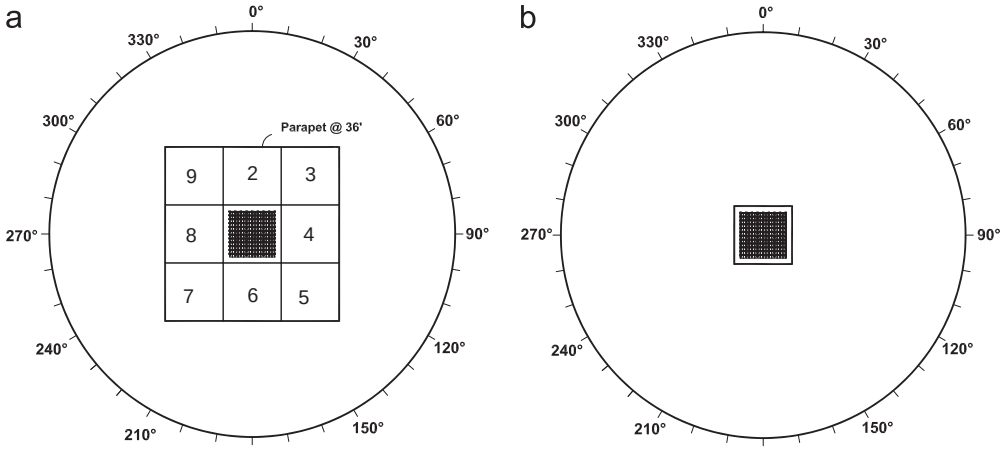

Fig. 4. Plan view of typical array layout for 6*H* model building (left) and 2*H* model building (right). In this case, the model scale is 1:50, and the roof height is 10 m at full scale. There is a 1 m tall parapet in this instance, though tests have been run with various parapet heights. Array locations used in the testing are numbered on the larger roof. The array is shown in location 1, the center of the roof. (a) 60 m × 60 m building and (b) 20 m × 20 m building.

Please cite this article as: Banks, D., The role of corner vortices in dictating peak wind loads on tilted flat solar panels mounted on large, flat roofs. Journal of Wind Engineering & Industrial Aerodynamics (2013), http://dx.doi.org/10.1016/j.jweia.2013.08.015

Fig. 5. Middle-of-the-roof test configuration. The array is rotated for testing every 10°. The building is not rotated. The goal of this test is to determine wind loads in a roof zone where the flow over the building edge has fully reattached to the roof surface.

information that tests can be designed and conducted which will reproduce these pressure patterns.

The effects of the vortices were found to dominate across the entire surface of the $6H \times 6H$ building described above. As it is common and desirable for solar racking manufacturers to install their products on the roofs of buildings that are much larger than this (it is not uncommon for roofs larger than $20H \times 10H$ to be largely covered in PV), we have also conducted tests on a $12H \times 6H$ roof in which the panels themselves are rotated, but the building is not, as illustrated in Fig. 5. This large building test was run with wind normal to the shorter building edge, so that persistent corner vortices never form. The goal of this test is to measure wind loads in a roof region where the flow over the edge of the building has fully reattached to the roof, and is flowing parallel to the roof surface. It is not the intent of these tests to characterize the loads for arrays skewed from the axis of the building; this would require testing of such skewed arrays beneath and near the vortices.

The convention used for defining wind directions in these tests is that the sun shines from 180° at midday, so that the panels are tilted with their lower edges on the 180° side. In the northern hemisphere, 180° is south. The dark side of the building, on which the sun does not shine (the north side in the northern hemisphere), is designated as 360°. While these wind direction conventions are consistent with the compass wind directions in the northern hemisphere, it is important to remember that it is the wind direction relative to the tilt of the panels which is being expressed in degrees. In all tests presented in this paper, the panels were aligned with the axis of the building.

Note that the GC_N values presented in the Results section do not represent the worst case values measured in all experiments. The wind loads varied with parameters such as the gap above the roof (h_2), the height above the roof (h_1), row spacing, and deflector design. The effect of these parameters merits a separate publication.

3. Results

Representative uplift pressure coefficients across individual solar panels for a typical 9-roof-region test are presented in Fig. 6. Before discussing what the zones of high lift (yellow and red) tell us, it is worth considering what is implied by the zones of low uplift (in blue/green).

3.1. The absence of roof-edge zones due to bubble separation

Looking at these images of the roof as seen from above, it is apparent that the edge separation bubbles are having very little impact. Uplift of the panels for wind directions of 0° and 90° are no different near the building edges than in the building interior. In these images, the panels were placed at an offset of roughly $0.2H$ from the roof's edge. Testing with the panels placed $0.03H$ from the roof's edge revealed the same pattern. The only evidence of any higher lift is due to the fact that low frequency lateral turbulence (i.e. momentary shifts in wind direction) occasionally causes weak corner vortices to form.

Winds from the sunny side (180°) cause a slight increase in uplift over a wide region extending between $1H$ and $3H$ from the roof's edge. This is inside the large recirculation beneath the bubble separation, and is likely because the air flow has reversed direction at the roof surface, and is flowing towards the high (dark) sides of the panels.

This means the only edge (non-corner) zone required for solar panels is a $3H$-wide zone along the sunny-side wall. This zone has comparatively mild uplift loads.

3.2. The critical nature of corner vortex effects

Four conical vortices form during the 180° sweep of wind directions presented in Fig. 6. These are labeled in Fig. 7, where Sw designates the vortex originating from a sunny-side corner with a weaker influence on uplift, Ds designates the dark-side corner vortex with the stronger uplift, etc. The expected position of the vortex core and reattachment are identified based on data from Banks et al. (2000) for a roof with no parapet. The parapet is expected to lift the vortex core higher off the roof surface, and for some wind directions to shift the vortex slightly (10–15%) further away from the roof edge (Banks, 2000).

We can see that for winds from 110° to 170°, two triangular swaths of yellow highlight the increased GC_N values associated with the two vortices that radiate from the corner in the lower right (vortex Ss and vortex Sw). The angle between each vortex and its corresponding roof edge increases as the wind becomes more perpendicular to that edge. Vortex Ss is seen to produce stronger uplift wind loads on the panels than vortex Sw, which has a weaker influence and only produces significant uplift on the exposed southern edge of the arrays in locations 3 and 4. In between the two vortex reattachment lines, there is a blue region where the panels are being pushed down into the roof. Downward forces on the panels can be significant. However, these loads are not examined in this paper.

The uplift forces for both of these vortices are greatest at a location that lies between the vortex core and the reattachment. In contrast, on the roof itself these vortices produce their highest suction forces directly beneath the vortex core (Banks et al., 2000).

When the winds originate from 10° to 80° (i.e. dark-side cornering winds), two vortices radiate from the upper right corner. Of the four vortices, vortex Ds clearly has the strongest impact on the panels. As is the case for vortex Ss, the swirling flow of this vortex is approaching the panels from behind their high sides, a condition that would be expected to cause higher lift. Unlike the two sunny-side corner vortices, the peak suction is beneath and even a little to the interior of the expected reattachment point. Conversely, vortex Dw produces a downforce under the reattachment, as the local flow direction along the roof surface is from the low side of the panels. Panels under the Dw vortex core saw a mild uplift in this case.

Fig. 8 shows a summary plot of the worst case loads for 0–90 and 90–180 for a different 10° tilt racking system with no deflector. The patterns are the same for most of the systems tested. As with vortex loads on the roof itself, the intensity of the uplift diminishes

Please cite this article as: Banks, D., The role of corner vortices in dictating peak wind loads on tilted flat solar panels mounted on large, flat roofs. Journal of Wind Engineering & Industrial Aerodynamics (2013), http://dx.doi.org/10.1016/j.jweia.2013.08.015

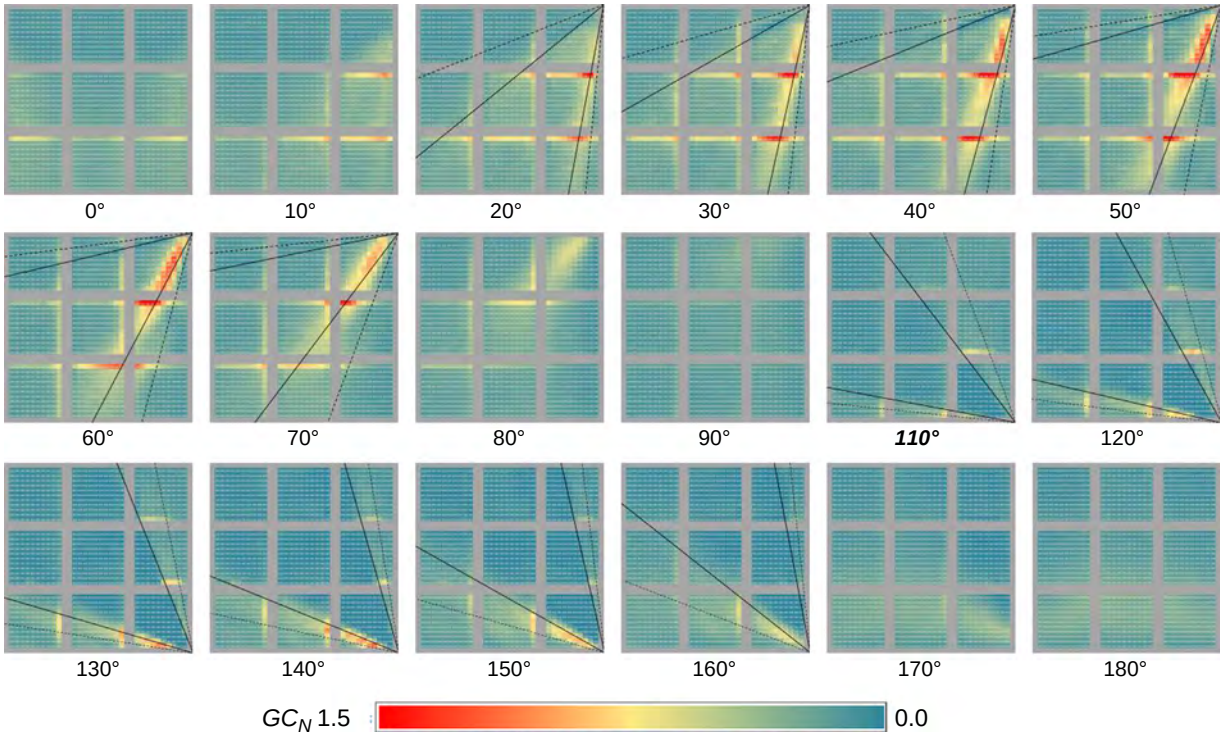

Fig. 6. Peak Uplift GC_N contours for 10° tilt, no wind deflector. Winds from 0° are from the top of the page (which is the dark side of the panels, north in the northern hemisphere), and winds from 90° are from the right hand side. Colors show GC_N from −1.5 (red) to 0.0 (blue). Values outside this range are clipped. Tributary area is one solar panel. Dashed black lines indicate anticipated average position of vortex cores for each wind direction, from Banks et al. (2000). Solid black lines indicate expected location of reattachment. (For interpretation of the references to color in this figure legend, the reader is referred to the web version of this article.)

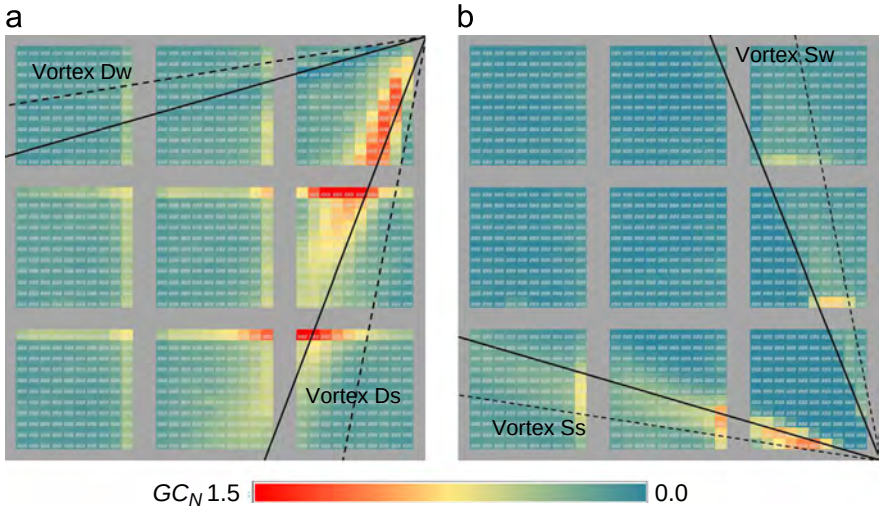

Fig. 7. Selected peak uplift contours from Fig. 6 with vortex identifier labels. (a) Wind direction 50° and (b) Wind direction 140°.

with distance from the corner at which the vortex originates. However, the width of the vortex increases with distance from the corner, so the number of panels seeing well-correlated loads goes up. This means that the benefits of load-sharing across several panels are less pronounced farther from the vortex origin.

3.3. Corner vortex effects on array edges

For unsheltered perimeter panels facing into the vortex, the uplift is significantly greater than for their counterparts in the array interior. This is illustrated in both Figs. 7 and 8. Recall that the arrays in each of the nine roof positions were tested separately, so that there were no upwind panels to disrupt the wind flow approaching along the roof surface.

As with the interior panels, the highest perimeter loads are attributable to vortex Ds. The north row of roof location 4 is experiencing loads that are 60–70% higher than what would be expected if there was a continuous array covering the whole roof surface. For roof location 5, the increase compared to the surrounding interior panels is more than a factor of 2. The effect of the vortices on edge panels does not decay as quickly as their effects on interior panels. In Fig. 8, there is no apparent effect of vortex Sw on interior panels in location 3. However, the south edge is clearly seeing higher uplift due the vortex.

Please cite this article as: Banks, D., The role of corner vortices in dictating peak wind loads on tilted flat solar panels mounted on large, flat roofs. Journal of Wind Engineering & Industrial Aerodynamics (2013), http://dx.doi.org/10.1016/j.jweia.2013.08.015

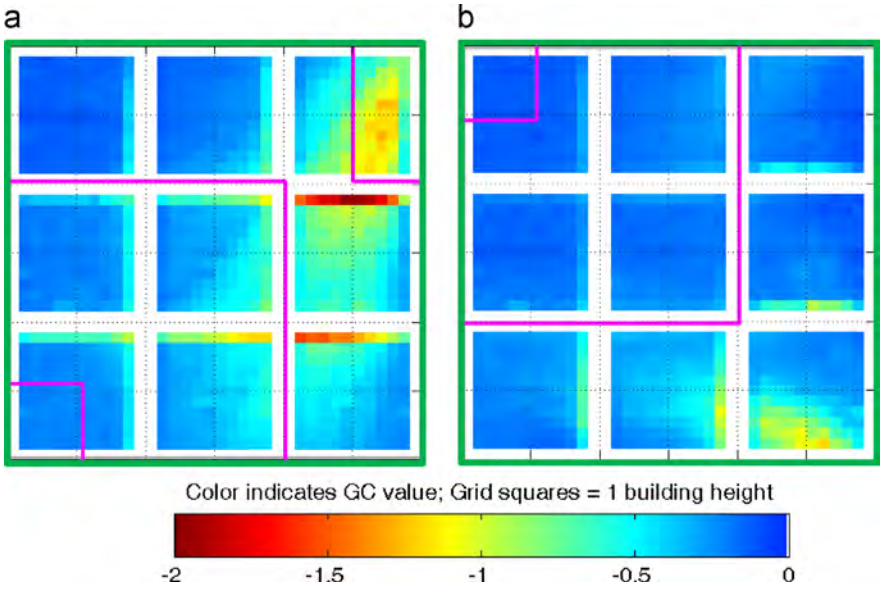

Fig. 8. Top view of GC_N contours for panels tilted at 10°. The racking system design is not identical to that of Fig. 6. The worst case for all wind directions is shown. Green lines represent the roof edge. Black dotted lines are $1H \times 1H$ squares. Pink line represent potential zone boundaries for roof-mounted solar. (a) Winds from 0° to 90° and (b) winds from 90° to 180°. (For interpretation of the references to color in this figure legend, the reader is referred to the web version of this article.)

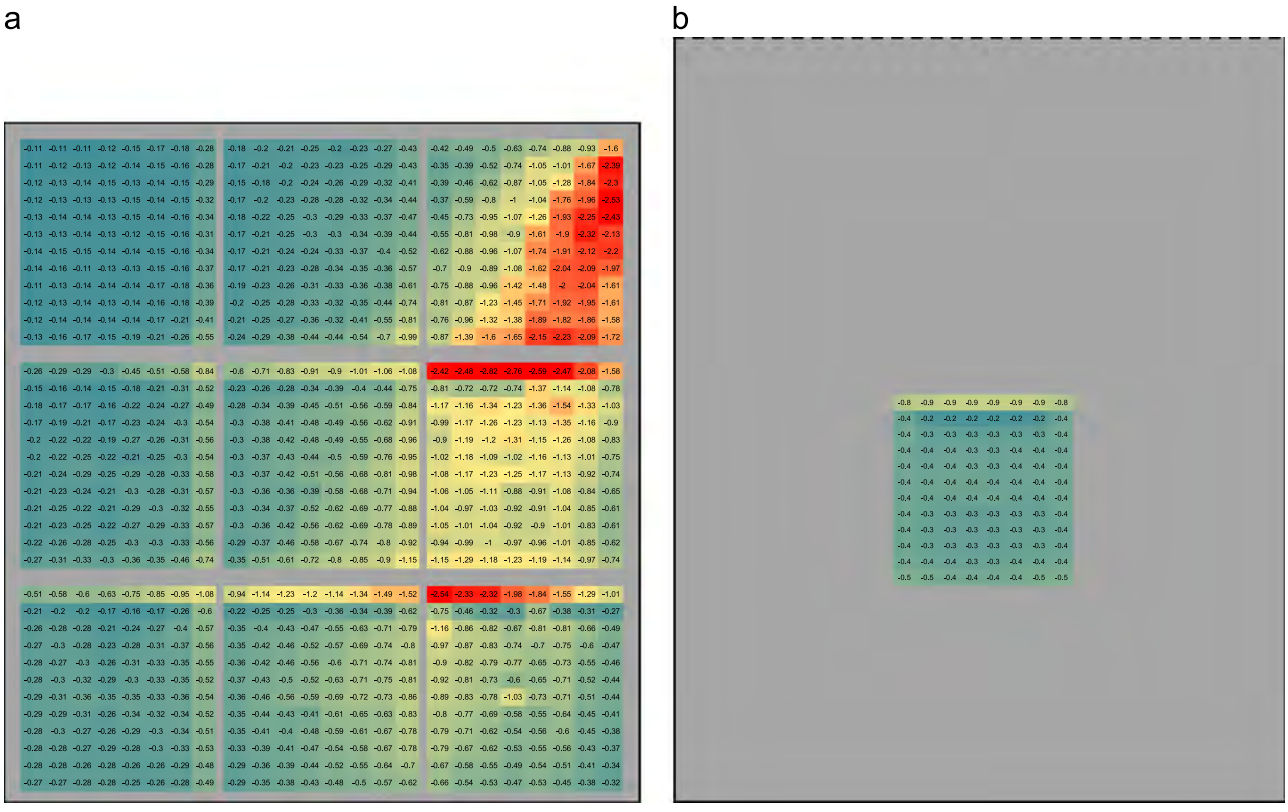

Fig. 9. Tilt = 10°, no deflector. (a) Worst case 9-roof-region GC_N values for winds from 0° to 90° relative to the building. and(b) Worst case GC_N from far middle-of-the-roof tests.

3.4. *The effect of building size*

Fig. 9 compares the results of the 9-zone, $6H \times 6H$ roof test with data from the rotating-array test on the longer $12H \times 6H$ roof (see Fig. 5). The goal of the long-roof test is to place the panels in a roof region that is not influenced by the corner vortices, and where the flow is fully reattached, and traveling along the roof surface.

Fig. 9(a) only includes data from wind directions from 0° to 90°, so the only vortices formed emanated from the upper right corner. Fig. 9(b) includes data from all array rotations, though the worst case loads primarily occurred for array rotations between 0° and 20°. For these particular racking systems, it is winds approaching from the higher north (dark) side of the array that create the highest loads. Pronounced north row edge effects are apparent in both images, along with sheltering of the second row from the north edge.

Please cite this article as: Banks, D., The role of corner vortices in dictating peak wind loads on tilted flat solar panels mounted on large, flat roofs. Journal of Wind Engineering & Industrial Aerodynamics (2013), http://dx.doi.org/10.1016/j.jweia.2013.08.015

Results from this kind of testing forms the basis for the zone 0 wind loads in SEAOC PV2. These far-middle roof loads were considered to define the edge of vortex-dominated zones 1, 2 and 3. Once loads drop below the zone 0 values, the vortex is no longer dictating the loads. It is clear that even in positions 5 and 6, more than 4*H* from the building corner and 2*H* from the building edge, the vortex is still creating loads much higher than what is seen in the far middle (zone 0).

Fig. 10 compares wind loads on identical arrays positioned on a $6H \times 6H$ building and on a smaller $2H \times 2H$ building. The worst per-panel uplift loads shown in the figure are reduced by a factor of 2 on the smaller roof.

Fig. 11 shows a similar comparison for critical wind directions for a different racking configuration. In this case the smaller $2H \times 2H$ building was tested both with and without the parapet. Once again, under the vortex Ds reattachment, the wind forces on the larger building are generally more than double those on the smaller one. The ratios for the other vortices are lower, but are still generally above 1.5.

The intensity of the vortices is dictated by the size of the object over which they are forming. By making the building three times wider, the vortex is made significantly stronger. For the range of building sizes tested in this study, the wind loads collapse well when PV tributary area is normalized by the frontal area of the building. It is not clear from our testing how wide a building must be before the vortex wind loads plateau near the vortex origin corners. Continued increase beyond 6*H* appears plausible.

While wider buildings have higher loads in the corner, the final column of Fig. 11 shows how low wind loads can be in the middle of a large roof, far enough from the corners that the corner vortices are not an issue. This was accomplished by rotating the array rather than the building (see Fig. 5).

3.5. The effect of parapets

The fact that the addition of a 1.2 m tall parapet to the 20 m × 20 m × 10 m building decreased uplift in Fig. 11 was a very unusual observation. A wide range of racking systems products were tested with and without parapets, and some results are presented in Fig. 12. The results from Fig. 11 provide the only data point in which the uplift force has decreased.

The only other case where the addition of a parapet decreases peak loads beneath the vortex is shown in Fig. 12b. The net effect of parapet is evidently somewhat different from vortex Ds to vortex Ss. However, the underlying vortex physics is the same. The parapet lifts the vortex up off the roof surface and shifts it away from the roof edge. Placing objects on the roof in the path of the vortex is known to disrupt and weaken the vortex (Surry and Lin, 1995). It is possible that as the vortex moves upward, the panels are less able to disrupt it, and loads increase accordingly. This trend is reflected in Fig. 12 by curve fit #1.

Once the parapets are high enough to form a kind of well on the rooftop, it is plausible that the vortices spin healthily but safely

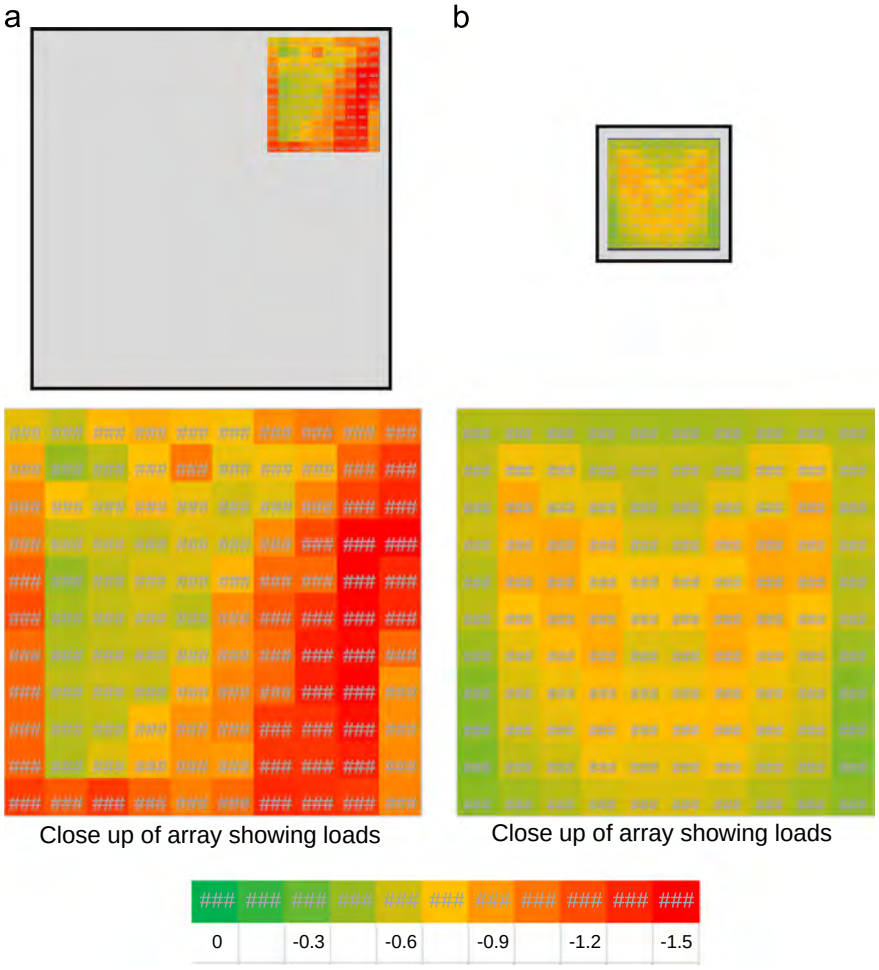

Fig. 10. Top view of array. Panels are tilted at 8°, with a deflector. 1-m (3 ft) tall parapet in place on both buildings. The GC_N contours are worst case values for all wind directions (0–350°, every 10°). Squares of color indicate load coefficients across a single solar panel. (a) Array location 3 on a $6H \times 6H$ roof and (b) same array covering $2H \times 2H$ roof, [see Fig. 4a and b]

Please cite this article as: Banks, D., The role of corner vortices in dictating peak wind loads on tilted flat solar panels mounted on large, flat roofs. Journal of Wind Engineering & Industrial Aerodynamics (2013), http://dx.doi.org/10.1016/j.jweia.2013.08.015

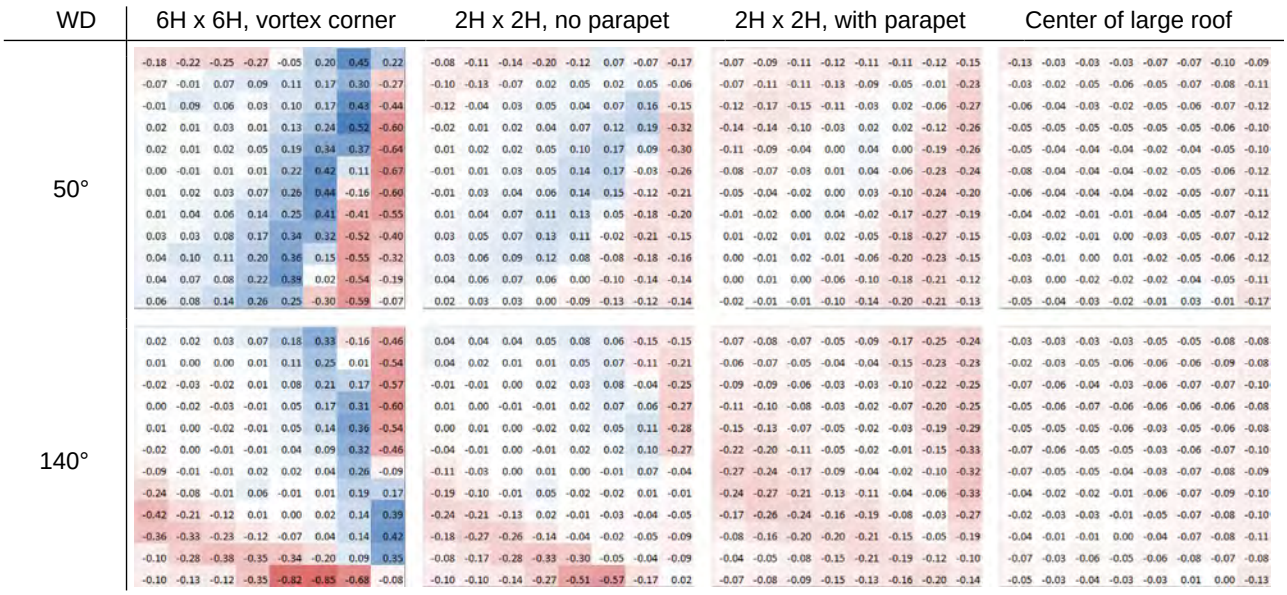

Fig. 11. Top view of array. Panels are tilted at 10°, with a deflector. 1.3-m tall parapet in place unless otherwise noted. Coloring indicates GC_N; blue is downforce, red is uplift. "Vortex corner" on $6h \times 6h$ building is location 5 for 140°, and location 3 for 50° (see Fig. 4a).

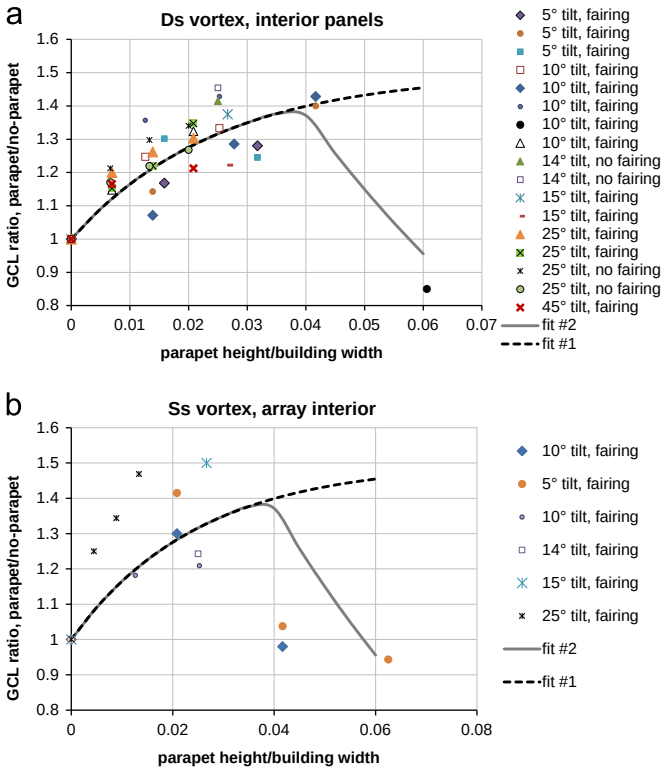

Fig. 12. Change in peak uplift as a result of the addition of a parapet. (a) Vortex Ds, interior (non-edge) panels only and (b) vortex Ss, interior (non-edge) panels only.

above the tops of the panels, and loads drop dramatically. This is thought to happen at around $h_{pt}/W > 4\%$, and is reflected in curve fit #2. Not enough data has been taken to define this threshold conclusively. A similar effect has been observed for wind loads on the roof itself, where for areas greater than 1 m^2, a low perimetric parapet increased peak roof suctions, but a parapets taller than 4% of the building width reduced loads (Kopp et al., 2005).

One other situation in which the parapets were observed to reduce loads is when panels that are shorter than the parapet are placed very close (offset $< h_{pt}$) to the parapet in the dark-side corner. This is at least in part due to the fact that the loads can be very severe for panels that jut out into the shear layer. None of the data presented in the figures in this paper are from panels positioned that close to a roof edge with no parapet. This situation has not been fully characterized, but all indications are that loads are quite high for panels in the shear layer.

Note that the load ratios in Fig. 12 do not generally represent loads on the exact same panel with and without the parapet. Since the location of the worst suction moves inward towards roof center when a parapet is added, the worst case loads from each configuration are compared, and this generally means different panels.

The parapet heights in Fig. 12 are normalized by the length of the building edge along with the vortex forms. The data was found to collapse slightly more effectively with this normalization than when normalized by building height or panel height, likely because of the roof-well effect described above. For very wide buildings, normalization by either roof height or some measure of wall size (such as sqrt(H*W)) is likely more appropriate.

Under any normalization method, there is still considerable scatter in this parapet effect the data, however. This is likely attributable to the considerable variation in the design and performance of the systems, most of which have deflectors. Since every data point is normalized by no-parapet performance, the results are quite sensitive to the peak values measured in this situation.

3.6. *The effect of wind deflectors or fairings*

Most of the data in Fig. 12 are from systems with wind deflectors (fairings) protecting their high (dark) sides from the wind. It is advised that any codification of wind loads on roof-mounted solar collectors not include a reduction factor for deflectors, because the effectiveness of these deflectors varied significantly between designs and locations on the roof. While deflectors nearly always decrease loads under vortex Ds, they will often increase wind loads under vortex Dw, and sometimes also under vortex Sw.

This paper is focused on uplift forces, but it is worth noting that the deflectors typically significantly increased the drag force, which is critical for the sliding mode of failure.

Please cite this article as: Banks, D., The role of corner vortices in dictating peak wind loads on tilted flat solar panels mounted on large, flat roofs. Journal of Wind Engineering & Industrial Aerodynamics (2013), http://dx.doi.org/10.1016/j.jweia.2013.08.015

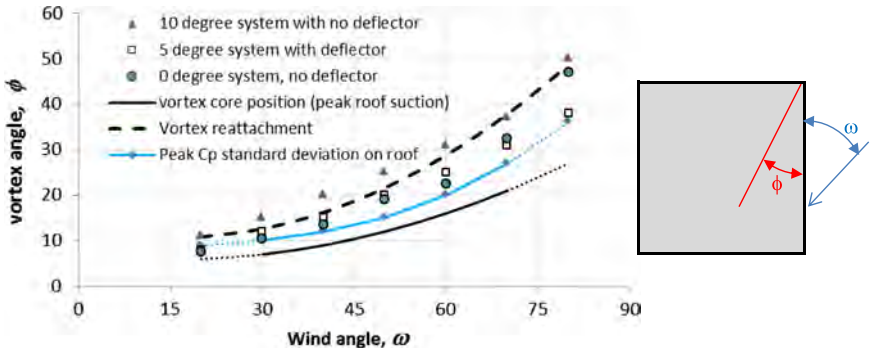

Fig. 13. Position of peak uplift on panels relative to vortex geometry for vortex Ds. Roof suction data from Banks et al. (2000). Figure on the right is a plan view of the roof. Wind direction relative to the relevant roof edge is ω, vortex angle relative to roof edge is ϕ.

4. Discussion

Banks et al. (2000) confirmed that the peak suction on the roof surface tracks the position of the vortex core, and illustrated that the peak standard deviation in the pressure roughly tracks just inside the vortex reattachment. This is because, in the zone between the peak suction and the reattachment, the suction on the roof is rapidly changing from a high uplift to a mild downforce. Since the angle of the vortex core relative to the roof edge is constantly changing, this region of the roof sees dramatic changes in pressure over short periods of time.

Having the highest net suction across the panels occur under the vortex core turns out to be a relatively rare situation. Fig. 13 shows that for tilts of 0°, 5° and 10°, the peak suction due to vortex Ds remains close to the reattachment. This is a little surprising, since away from the array edges, the 5° system with a deflector and the 0° system can both be considered to see high loads due to lapses in pressure equalization, rather than as a result of the swirling vortex catching the high side of the panels. These peak uplift values are just inside the vortex reattachment, in a region where the roof suction is rapidly changing both spatially and temporally. This suggests that the pressure equalization is fairly effective under the vortex core, but has trouble adjusting to the sudden and drastic changes in pressure between the vortex core and the reattachment.

This suggests that for roof mounted solar panels, using zones intended for the roof itself (such as the ASCE 7 components and cladding zones) is not appropriate, since the roof-load zones are based on the vortex core location, and the solar panel zones are based on the position of the reattachment, nearly twice as far into the roof. The testing has shown consistently that the worst case uplifts for a wide range of systems occurs under the vortex Ds reattachment at a location between 0.8H and 1.2H from the 0° (dark side) edge and 0.6–0.8H from the east or west edge. These values are well in excess of the typical building roof edges zones, such as the 0.4H used for cladding loads in ASCE 7.

Fig. 6 shows the uplift patterns for wind directions from 0° to 180°. Of course, evidence of four similar vortices would appear, mirrored on the left side of the roof images, if testing were performed for wind directions from 190° to 350°. It is clear that there is no part of a $6H \times 6H$ roof where the loads are not dictated by the vortices. The effects of vortex Ds alone are significant across the entire roof surface.

One implication of this result is that any roof-top solar wind load calculation method that does not consider the position and orientation of the panels relative to the corner vortices is a method that neglects the fundamental physics driving the loads.

All of the testing in this study has been performed on an isolated rectangular building. It is likely that in practice loads measured on this building shape are conservative for most installations, since most changes to the corner geometry will weaken the vortex. The addition of a corner stairwell jutting out from the wall and/or above the roof or the presence of an attached low-rise at the base is an example. However, it is possible that some changes will increase loads. It is not clear that a 90° corner angle provides the strongest vortex, or how strong the vortex effects will be on L-shaped or U-shaped buildings.

It is also possible that loads will continue rising as building width increases beyond 6H, though the loads must plateau at some width.

All of the testing has been conducted with uniform parapets surrounding the entire roof perimeter. If one of the sides does not have a parapet, then the well effect is lost, and the sudden decrease in wind loads for taller parapets is much less likely. It should also be noted that uneven parapets can reduce the intensity of the vortex, as has been observed for sawtooth parapets (Surry and Lin, 1995).

5. Conclusions

The most significant loads on roof mounted solar are consistently observed for wind directions that form corner vortices. As a corner vortex swings out across the roof with changing wind direction, so does the position of peak uplift on the panels, and it does so at an angle known to correspond to the location of the vortex reattachment. From this one can conclude that these peak uplift loads are related to the interaction of the corner vortices with the panels. The absence of any significant loading under the edge separation bubble, and the significantly lower loads observed for arrays located in fully reattached flows, indicates that the most critical loads on roof mounted solar are dictated by the corner vortices.

For a 6H-wide building, the peak uplift wind loads were observed more than 1H from the roof corner. This distance is significantly greater than that expected for peak vortex-related loads on the roof itself. This is because these peak wind loads were typically observed for panels under the vortex reattachment, rather than under the vortex core, as is the case for the roof itself. As a result, roof zones based on (and intended for) wind loads on the roof surface itself are not suitable for wind loads on tilted roof mounted solar panels, as they do not extend far enough into the roof.

Another difference between the load patterns on the roof itself and those on tilted roof mounted solar panels is that the load patterns for the latter demonstrate considerable asymmetry. For northeast cornering winds, the uplift loading on panels along the east edge of the roof is much more severe than for panels along the north edge. Conversely, for southeast cornering winds, the loading of panels along the south roof edge is much more severe than along the east roof edge. From this it can be concluded that the relationship

Please cite this article as: Banks, D., The role of corner vortices in dictating peak wind loads on tilted flat solar panels mounted on large, flat roofs. Journal of Wind Engineering & Industrial Aerodynamics (2013), http://dx.doi.org/10.1016/j.jweia.2013.08.015

between the direction of the panel tilt and the swirl of the vortex is very significant. This is the reason why caution should be used in trying to apply these results to panels which are not mounted in arrays aligned with the building edges.

These tests included solar arrays positioned with array offsets from the roof edge greater than two building heights ($>2H$). When such arrays are positioned near the vortex, significantly higher uplift wind loads were consistently observed for panels located along the edges of these arrays when compared with nearby sheltered interior panels. The highest uplift loads were observed for panel edges facing into the roof corner from which the vortex originates. Edge factor multipliers of 1.5 and 2.0 were common.

Appreciably more severe wind loads were observed for larger aspect ratio buildings than for smaller ones of the same height, and common parapet heights were observed to increase wind loads by 20–30% as compared to no-parapet tests. Since the vortices control the wind load on tilted flat-panel roof-mounted PV, it is expected that these changes to the building geometry have enhanced the strength of these vortices.

Acknowledgments

Dave Carpenter, Scot Waye, and Yarrow Fewless deftly managed the multitude of experiments and made elegant synopses of the mountains of data. This paper would not have been possible without them.

References

ASCE 7-10, ASCE, 2010. Minimum design loads for buildings and other structures. American Society of Civil Engineers, Reston, VA.

Banks, D., Meroney, R.N., Sarkar, P.P., Zhao, Z., Wu, F., 2000. Flow visualization of conical vortices on flat roofs with simultaneous surface pressure measurement. Journal of Wind Engineering and Industrial Aerodynamics. 84, 65–85.

Banks, D, 2000. The suction induced by conical vortices on low-rise buildings with flat roofs. Ph.D. Dissertation. Civil Engineering Department, Colorado State University, Fort Collins, CO.

Banks, D, 2011. Measuring Peak Wind Loads on Solar Power Assemblies. In: Proceedings of the 13th International Conference on Wind Engineering. 11th–15th July, Amsterdam, The Netherlands.

Dyrbye, C., Hansen, S., 1997. Wind Loads on Structures. Wiley & Sons, Chichester, England.

Kind, R.J., 1986. Worst suctions near edges of flat rooftops on low-rise buildings. Journal of Wind engineering and Industrial Aerodynamics 25, 31–47.

Kopp, G.A., Wind loads on low profile, tilted, solar arrays placed on large, flat, low-rise building roofs, ASCE Journal of Structural Engineering, http://dx.doi.org/10.1061/(ASCE)ST.1943-541X.0000825, in press.

Kopp, G.A., Banks, D., 2013. Use of the wind tunnel test method for obtaining design wind loads on roof-mounted solar arrays. Journal of Structural Engineering 139 (2), 284–287.

Kopp, G.A., Surry, D., Mans, C., 2005. Wind effects of parapets on low buildings: Part 1. Basic aerodynamics and local loads. Journal of Wind Engineering and Industrial Aerodynamics, 93, 817–841.

Kopp, G.A., Farquhar, S., Morrison, M.J., 2012. Aerodynamic mechanisms for wind loads on tilted, roof-mounted, solar arrays. Journal of Wind Engineering and Industrial Aerodynamics 111, 40–52.

Richards, P.J., Hoxey, R.P., Connell, B.D., Lander, D.P., 2007. Wind tunnel modelling of the Silsoe cube. Journal of Wind Engineering and Industrial Aerodynamics 95, 1384–1399.

SEAOC 2012. Wind design for low-profile solar photovoltaic arrays on flat roofs. SEAOC Report PV2-2012, Structural Engineers Association of California, Sacramento, California.

Surry, D., Lin, J.X., 1995. The effect of surroundings and roof corner geometric modifications on roof pressures on low-rise buildings. Journal of Wind Engineering and Industrial Aerodynamics 58, 113–138.

Please cite this article as: Banks, D., The role of corner vortices in dictating peak wind loads on tilted flat solar panels mounted on large, flat roofs. Journal of Wind Engineering & Industrial Aerodynamics (2013), http://dx.doi.org/10.1016/j.jweia.2013.08.015